Redox Biology 49 (2022) 102210

Contents lists available at ScienceDirect

Redox Biology

journal homepage: www.elsevier.com/locate/redox

Implication of type 4 NADPH oxidase (NOX4) in tauopathy

Enrique Luengo [a,b,1], Paula Trigo-Alonso [a,b,1], Cristina Fernández-Mendívil [a,b], Ángel Nuñez [c], Marta del Campo [d], César Porrero [c], Nuria García-Magro [c,e], Pilar Negredo [c], Sergio Senar [f], Cristina Sánchez-Ramos [g], Juan A. Bernal [g], Alberto Rábano [h], Jeroen Hoozemans [i], Ana I. Casas [j,k], Harald H.H.W. Schmidt [j], Manuela G. López [a,b,*]

[a] Instituto Teófilo Hernando for Drug Discovery, Department of Pharmacology, School of Medicine, Universidad Autónoma de Madrid, Madrid, Spain
[b] Instituto de Investigación Sanitario (IIS-IP), Hospital Universitario de la Princesa, Madrid, Spain
[c] Department of Anatomy, Histology and Neuroscience, School of Medicine, Universidad Autónoma de Madrid, Madrid, Spain
[d] Department of Health and Pharmaceutical Science, Faculty of Pharmacy, San Pablo CEU University, Montepríncipe, Alcorcón, Spain
[e] Facultad de Ciencias de la Salud, Universidad Francisco de Vitoria, Pozuelo de Alarcón, Madrid, Spain
[f] Dr. Target Machine Learning. Calle Alejo Carpentier 13, Alcala de Henares, 28806, Madrid, Spain
[g] Myocardial Pathophysiology Area, Centro Nacional de Investigaciones Cardiovasculares (CNIC), Madrid, Spain
[h] Department of Neuropathology and Tissue Bank, Unidad de Investigación Proyecto Alzheimer, Fundación CIEN, Instituto de Salud Carlos III, Madrid, Spain
[i] Department of Pathology, Amsterdam University Medical Centers Location VUmc, Amsterdam, the Netherlands
[j] Department of Pharmacology and Personalized Medicine, Maastricht Center for Systems Biology, Faculty of Health, Medicine and Life Sciences, Maastricht University, Maastricht, the Netherlands
[k] Department of Neurology, University Hospital Essen, Essen, Germany

ARTICLE INFO

Keywords:
Alzheimer's disease
Tauopathy
Autophagy
NADPH oxidases
NOX4

ABSTRACT

Aggregates of the microtubule-associated protein tau are a common marker of neurodegenerative diseases collectively termed as tauopathies, such as Alzheimer's disease (AD) and frontotemporal dementia. Therapeutic strategies based on tau have failed in late stage clinical trials, suggesting that tauopathy may be the consequence of upstream causal mechanisms. As increasing levels of reactive oxygen species (ROS) may trigger protein aggregation or modulate protein degradation and, we had previously shown that the ROS producing enzyme NADPH oxidase 4 (NOX4) is a major contributor to cellular autotoxicity, this study was designed to evaluate if NOX4 is implicated in tauopathy. Our results show that NOX4 is upregulated in patients with frontotemporal lobar degeneration and AD patients and, in a humanized mouse model of tauopathy induced by AVV-Tau^{P301L} brain delivery. Both, global knockout and neuronal knockdown of the *Nox4* gene in mice, diminished the accumulation of pathological tau and positively modified established tauopathy by a mechanism that implicates modulation of the autophagy-lysosomal pathway (ALP) and, consequently, improving the macroautophagy flux. Moreover, neuronal-targeted NOX4 knockdown was sufficient to reduce neurotoxicity and prevent cognitive decline, even after induction of tauopathy, suggesting a direct and causal role for neuronal NOX4 in tauopathy. Thus, NOX4 is a previously unrecognized causative, mechanism-based target in tauopathies and blood-brain barrier permeable specific NOX4 inhibitors could have therapeutic potential even in established disease.

1. Introduction

Aggregates of tau protein characterize several neurodegenerative diseases (NDDs) collectively known as tauopathies, which include Alzheimer's disease (AD) and Frontotemporal lobar dementia (FTLD), among others [1]. In spite of their prevalence and social-economic burden, there is still no effective therapy to cure or detain them. Therefore, there is an urgent need to find new and effective therapeutic targets for these diseases.

The major pathways that favor tau clearance include the ubiquitin-proteasome system and the autophagy-lysosomal pathway (ALP) [2]. Among the different autophagy types, macroautophagy is a major intracytoplasmic protein degradation pathway characterized by the formation of double-membraned vesicles called autophagosomes that

* Corresponding author. Department of Pharmacology, School of Medicine-UAM, Calle Arzobispo Morcillo 4, 28029, Madrid, Spain.
E-mail address: manuela.garcia@uam.es (M.G. López).
[1] These authors contributed equally.

https://doi.org/10.1016/j.redox.2021.102210
Received 28 June 2021; Received in revised form 30 November 2021; Accepted 8 December 2021
Available online 10 December 2021

engulf cargo and target it to the lysosome for degradation and elimination of damaged organelles and large protein aggregates [3–5]. ALP impairment in being recognized in the pathogenesis of AD [6–8]. Considering that tau is degraded via autophagy [2], dysfunction of ALP could lead to increased levels of its aggregated and toxic oligomeric forms [9]. Tau can also inhibit autophagic degradation, disrupt autophagosome dynamics and induce lysosomal alterations, contributing to tau-induced toxicity [10], which strongly relates to synaptic and cognitive deficits [11]. All these evidences suggest that once tau aggregates are present in neurons, pathology can become self-perpetuating. Thus, given the involvement of defective autophagy in the pathogenesis and progression of tauopathies such as AD or FTLD, therapies based on autophagy regulation can be implemented as ALP modulation accelerates degradation of tau protein aggregates [6,12,13].

Autophagy can be regulated by reactive oxygen species (ROS) [14–16]. NADPH oxidases (NOXs) are considered the major enzymatic sources of ROS production [17] and NOX-derived ROS have been reported as autophagy regulators [18,19]. Among the members of this seven-member family, NOX4, one of the main isoforms expressed in the central nervous system (CNS) [20], was found to regulate autophagy in energy-deprived cells [19]. NOX4 may be a key participant in the increased NOXs activity reported in AD progression as its expression is significantly increased in the brain of aged humanized APPxPS1 double transgenic mice [21]. In line with this, we have recently demonstrated that neuronal NOX4 is a major contributor to cellular autotoxicity upon ischemia or hypoxia [22]. In addition, neuronal NOX4 has been implicated in the progression of Parkinson's disease (PD) [23] and Traumatic Brain Injury (TBI) [24,25]. Also, several studies have reported the involvement of NOXs in cognitive dysfunction in AD patients and in *in vivo* AD models [21,26,27]. While NOX4 has been involved in amyloid beta (Aβ)-related AD models [21,28] its implication with tau protein, the main driver of toxicity in AD, is currently unclear. Here, we aim to determine the potential implication of NOX4 in tau pathology and whether NOX4 inhibition could be validated as a novel therapeutic strategy to treat tauopathies.

2. Materials and methods

2.1. Animal usage and care

Three-to-five-months-old C57BL/6n NOX4 knockout ($NOX4^{-/-}$) and littermates wild-type ($NOX4^{+/+}$) male/female mice (25–30 g) were used. They were maintained in a conventional animal facility on a 12 h light/12 h dark cycle, with food and water *ad libitum*. $NOX4^{-/-}$ mice were generated by deleting the NADPH and FAD binding sites of NOX4 that are essential for its activity as previously described [29]. $NOX4^{+/+}$ and $NOX4^{-/-}$ used in this study were genotyped (Supplemental Materials and Methods and Supplemental Fig. 1A) and characterized by immunofluorescence in Supplemental Fig. 1B and C.

2.2. Post mortem brain tissue

Hippocampal and prefrontal cortex frozen postmortem samples from FTLD and AD patients and non-demented controls were obtained from the Brain Tissue Bank of Fundación CIEN (Madrid, Spain). These samples were used for RNA and protein extraction. For immunohistochemistry, fixed hippocampal tissue in paraformaldehyde (PFA) from FTLD, AD and control subjects were obtained from the pathology department of VUmc and the Netherlands Brain Bank (Amsterdam, the Netherlands). Characteristics of subjects are summarized in Supplemental Table 1.

2.3. Study approval

All procedures involving animals were performed following the Guide for Care and Use of Laboratory Animals and approved by the Institutional Ethics Committee of Universidad Autónoma de Madrid and the Comunidad Autónoma of Madrid, Spain, (PROEX 252/16 and PROEX 218.5/20) following the European Guidelines for the use and care of animals for research in accordance with the European Union Directive of September 22, 2010 (2010/63/UE) and with the Spanish Royal Decree of February 1, 2013 (53/2013). All efforts were made to minimize animal suffering and to reduce the number of animals used. The Ethics Committee of the Hospital La Paz, Madrid, Spain and the Brain Tissue Bank of Fundación CIEN approved all protocols for experimental procedures in human samples (Ref HULP PI-3380 and S18007, respectively). Written informed consent was obtained from all subjects.

2.4. Adeno-associated viral vectors

Adeno-associated viral (AAV) vectors 2/6-SYN1-EGFP (**GFP**) and AAV2/6-SYN1-humanTau^{P301L} (**hTau**) were produced and purified as previously described [30]. For *in vivo* neuronal NOX4 knockdown, AAV9-shRNANOX4-EGFP (**shNOX4**) and AAV9-shSCR-EGFP (**shSCR**) were purchased from VectorBuilder (Chicago, USA).

2.5. Animal surgery and tauopathy model

Tauopathy was induced by intracerebroventricular (ICV) delivery of hTau vectors as described by Luengo et al. [30]. AAV-GFP ICV injected mice were used as control. Mice were anesthetized with Isoflutek (Isofluorane 1000 mg/g) in oxygen under spontaneous respiration (induction at 5% and maintenance at 2%). For the *in vivo* NOX4 neuronal knockdown, intrahippocampal injections (IHP) of 1.01 μL ($>10^{12}$ GC/mL) of AAV-shNOX4 or AAV-shSCR were injected (0.1 μL/min) in the right hemisphere following the same method as described by Luengo et al. [30] but using different coordinates (A: −1.94; L: −1.4; V: 1.8 mm, from Bregma). After surgery, mice were housed for postoperative monitoring and kept until the end of the experiment (day 28). At day 28 post-surgery mice were sacrificed, under 5% isoflurane anesthesia, by decapitation.

2.6. Real-time quantitative Polymerase Chain Reaction (RT-qPCR)

Total RNA from human hippocampal and prefrontal cortex tissue and mouse tissues (hippocampus, kidney and lung) was extracted with TRIzol reagent (Sigma-Aldrich) and 1 μg was reverse-transcribed using PrimeScriptTM RT Reagent Kit (perfect Real Time) (Takara). RT-qPCR was performed with qPCRBIO SyGreen Mix LoRox polymerase (Cultek) in a 7500 Fast Real-Time PCR System (Applied Biosystems by Life Technologies). Thermal cycling was carried out according to the manufacturer's recommendations, and the relative expression levels were calculated using the comparative ΔΔCt method. The primers were obtained from Sigma-Aldrich, Madrid, Spain, (Supplemental Table 2).

2.7. Measurement of insoluble and soluble fractions of hippocampal tissue

The protocol followed to obtain the sarkosyl-soluble (SS) and sarkosyl-insoluble fractions (SI) was performed as previously described with some modifications [31] Tissues were homogenized in A Buffer (Supplemental Materials and Methods) and centrifuged at 20.000 rpm for 20 min at 4°C. To obtain the SI fractions, pellets were resuspended in RAB buffer 1% sarkosyl (Supplemental Materials and Methods). Then, samples were vortexed for 1 min at room temperature, rotated at 4°C overnight and centrifuged at 69.000 rpm for 30 min at 4°C. SS fractions were collected from the supernatants and SI fractions, from the pellets, which were resuspended in RAB buffer 1% sarkosyl.

2.8. Western blotting

Tissues were lysed in 150 μL of ice-cold AKT lysis buffer (Supplemental Materials and Methods). 20 μg of SS, SI and protein extracts from

human and mouse samples were resolved in SDS-PAGE transferred to Immobilon-P PVDF membranes (Millipore). Membranes were activated with methanol and blocked with 4% bovine serum albumin (BSA) in Tris-buffered saline-Tween (TTBS) for 2 h and then incubated with the primary antibody (Supplemental Table 3). Then, washed thrice with TTBS and incubated with appropriate peroxidase-conjugated secondary antibody (1:10.000; Santa Cruz Biotechnology) for 45 min. Thereafter, membranes were washed thrice with TTBS, incubated with ECL-Advance Western-blotting Detection Kit (GE Healthcare), exposed using a ChemicDoC MP System (Bio-Rad Laboratories) and specific immunoreactive bands were quantified using Fiji software.

2.9. Immunofluorescence

At final point, mice were deeply anesthetized with sodium pentobarbital and perfused through the ascending aorta with 0.9% NaCl, followed by 30 mL of 4% PFA in 0.1 M phosphate buffer (PB, pH 7.4). Brains and kidneys were removed, post-fixed in the same fixative at 4°C overnight, and cryoprotected for 2 days in 30% sucrose. Forty-micrometer coronal slices were cut using a sliding microtome. For immunofluorescence assays, sections or fixed cells were abundantly washed with PB 0.1 M. Then, slices were blocked in PB 0.1 M with 2% Triton and 10% goat or donkey serum for 1 h, and incubated with the selected primary antibody (Supplemental Table 3) overnight at 4°C. In the neuronal cultures, cells were washed with PB 0.1 M. 0.1% Triton (2 × 5 min each), blocked with 0.1% Triton, 10% goat serum and BSA for 1 h, and incubated in 0.1% Triton, 5% goat serum and BSA with the primary antibody (Supplemental Table 3) overnight at 4°C. Tissue sections and cells were incubated with the appropriate secondary antibodies (Alexa Fluor 488, 546, 647; Invitrogen) for 1 h and 30 min at 1:200 or 1:800, respectively, and then washed with PB 0.1 M (3 × 5 min each). In the second wash, Hoechst (33342, Invitrogen) (1 μg/mL) was added.

Human brain tissue sections were de-paraffinized in xylene and rehydrated in decreasing gradients of ethanol solutions. Afterwards, antigen retrieval was performed by transferring sections to sodium citrate buffer (pH 6.0) at 60 °C for 20 min. Sections were then allowed to cool down for 15 min, and preincubated for 2 h at room temperature in a blocking solution of tris-buffered saline 0.1 M containing 10% goat serum and 0.3% Triton. Sections were then incubated with primary antibodies (Supplemental Table 3), diluted in blocking solution overnight at 4 °C, and washed and incubated with the appropriate secondary antibodies for 1 h and 30 min prior to washing and mounting. Brain sections or fixed primary cell cultures were mounted and covered. All images were taken in a SP5 confocal microscope (TCS SPE; Leica) and processed and analyzed with Fiji software.

2.10. Neuronal layer thickness measurement

Hoechst–stained sections were used to measure the cell layer thickness. Hippocampal sections from similar coordinates were selected. The thicknesses of the retrosplenial cortex (CTX), CA1 and the top granule cell layer in the dentate gyrus (DG TOP) were measured by drawing a scale perpendicular to the cell layer. Three different measurements from three different images acquired per mice were analyzed and represented as mean thickness.

2.11. In vivo recordings of long-term potentiation

Mice were anesthetized with urethane (1.6 g/kg) and body temperature maintained at 37 °C. Electrodes were placed stereotaxically according to the Paxinos and Franklin (2003) atlas. Field potentials were recorded through tungsten macroelectrodes (1 MΩ) placed at the CA1 region (A: −2.2; L: −1.5; V: 1–1.5 mm, from Bregma). Bipolar stainless-steel stimulating electrodes were aimed at the Schaffer collateral (SC) pathway of the dorsal hippocampus (A: −2.2; L: −2.5; V: 2 mm, from Bregma) to evoke CA1 responses. Field potentials were amplified (DAM80; World Precision Instruments, Florida, USA), bandpass filtered between 0.1 Hz and 1.0 kHz, and digitized at 3.0 kHz (CED 1401 with Spike 2 software; Cambridge Electronic Design). SC fibers were continuously stimulated with single pulses (50–200 μA, 0.3 ms, 0.5 Hz). LTP was evoked by theta-like burst stimulation (TBS) protocol, which consisted in three trains of stimuli (50 Hz, 200 ms duration), with a time-lag between trains of 200 ms (5 Hz; to mimic hippocampal theta activity). Field excitatory postsynaptic potentials (fEPSPs) were recorded during 20 min of control period and 30 min after a TBS. The initial slope of the fEPSP was assessed to quantify long-term changes of synaptic transmission. The average response during 1 min was calculated. The mean average response during the 20 min period before the tetanic stimulation was considered as 100%.

2.12. Behavioral tests

For assessing recognition memory, the novel object recognition test (NOR) was performed [32]. To assess spatial memory, the object location task (OLT) [33] and the T maze were conducted; the latter with some modifications [34]. Briefly, mice were placed in the start area of the maze with guillotine doors raised and the central partition placed. The mouse was confined in the chosen arm for 1 min by sliding the door down. After this, the mouse was placed in the start area with the guillotine doors opened and the central partition removed. The test was performed seven consecutive times and a correct response was considered when the animal chose the arm that was not entered before.

2.13. Primary neuronal culture and treatments

Primary neuronal cultures were prepared from P0 C57BL/6n $NOX4^{+/+}$ and $NOX4^{-/-}$ mouse embryos as previously described [35]. Briefly, pups were sacrificed, and the brains were extracted and placed in Hank's buffered salt solution. Meninges were removed and cortical and hippocampal tissue isolated, digested with papain (Sigma-Aldrich; diluted in Neurobasal (Invitrogen), DNase I (Sigma-Aldrich) (2 units/mL), EDTA (0.5 mM) and, activated with L-cysteine (Sigma-Aldrich) (1 mM) at 37 °C. Afterwards, the tissue was mechanically dissociated in feeding medium (Supplemental Materials and Methods) and once centrifugated, the cell pellet was resuspended in feeding medium supplemented with 8% Fetal Bovine Serum (Sigma-Aldrich) and filtered through a 70 μm cell strainer (Corning). Neurons were plated onto 18 mm diameter coverslips previously treated with HCl 1 M, bathed with ethanol and coated with poly-D-lysine (Sigma-Aldrich) (0.2 mg/mL in borate buffer) and 1 h after feeding, medium was replaced by fresh feeding medium. Neuronal cultures were maintained at 37°C in 5% CO_2. Beginning on day 4 *in vitro*, feeding media was supplemented with 200 μM D, L-aminophosphonovalerate (APV) (Abcam), and feeding medium was repeated with 100 μM APV every 4 days.

At day 14, neurons were treated with AAV-hTau or PBS (control) and maintained up to 22 days in culture. Additionally, for visualization of dendritic spines, neurons were treated at day 14 with AAV-GFP. To monitor autophagosome and autophagolysosome formation, the Premo™ Autophagy Tandem Sensor RFP-GFP-LC3B Kit (Termofisher) was added to the neuronal cultures 48 h before fixation. Neurons were then fixed at day 22 in 2% paraformaldehyde for 15 min.

Composition of buffers, culture media and solutions are in Supplemental Materials and Methods.

2.14. Statistics

Data are presented as mean ± SEM. All statistical tests were performed with GraphPad (GP) Prism (version 8.3.0). Data were tested for normality to determine the use of non-parametric or parametric tests. Unless otherwise noted, all grouped comparisons were made by one-way ANOVA with Tukey's correction and all pairwise comparisons by two-sided Student's t-tests, depending on the experimental design.

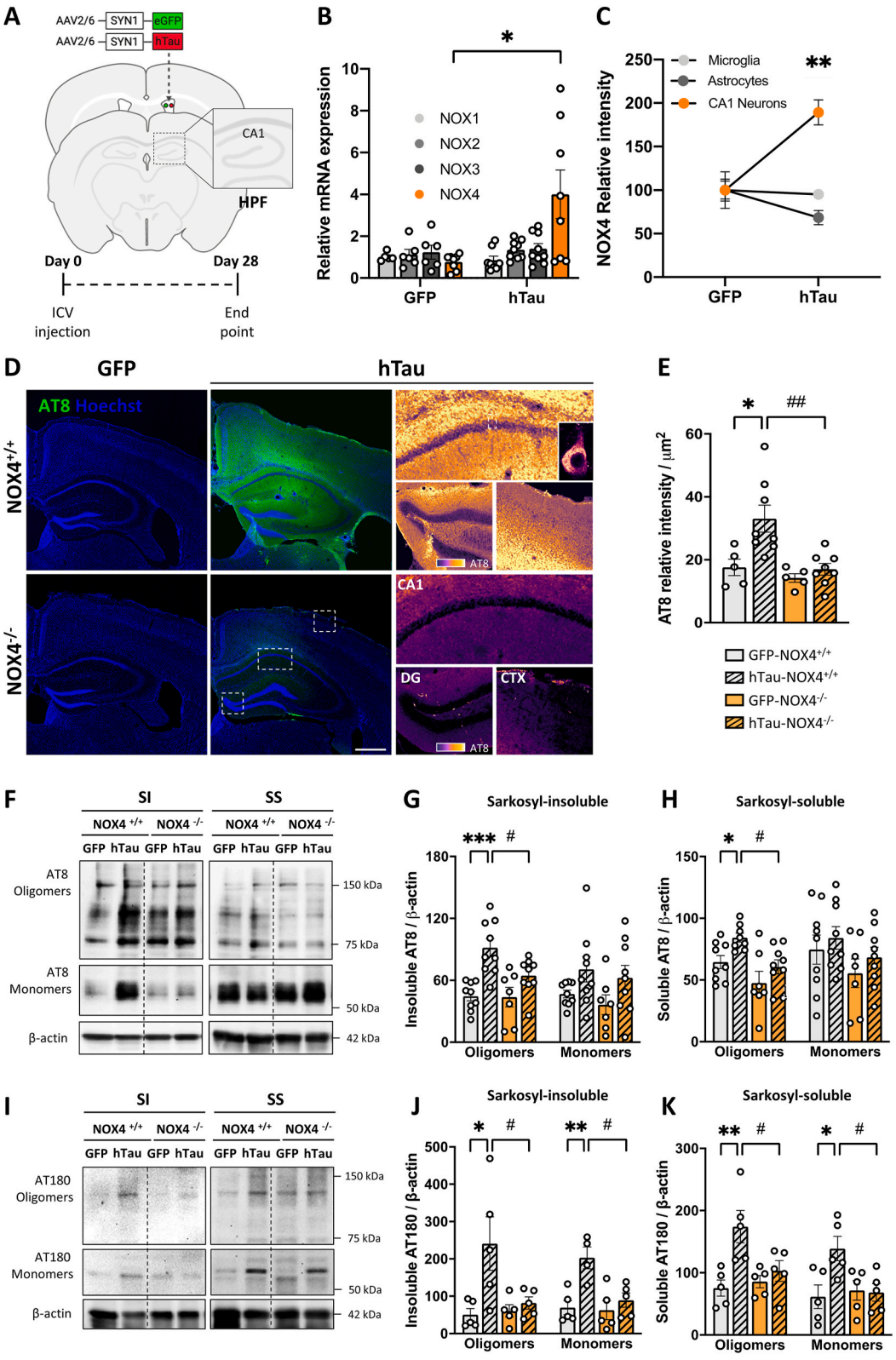

Fig. 1. NOX4 is upregulated after hTau injection and NOX4 genetic deletion reduces tauopathy 28 days after hTau injection. **(A)** Schematic representation of the protocol. (**B**) mRNA levels of NOX isoforms in hippocampal lysates from GFP (n = 5–8) and hTau (n = 8–9) injected mice. **(C)** NOX4 relative intensity in hippocampal CA1 neurons, microglia and astrocytes from GFP (n = 3–6) and hTau (n = 3–7) injected mice. (**D**) Representative images and **(E)** quantification of AT8 relative intensity in the hippocampus from NOX4$^{+/+}$ (GFP, n = 5 and hTau, n = 8) and NOX4$^{-/-}$ (GFP, n = 5 and hTau, n = 8) mice. Insets show images at a higher magnification. Scale bar: 500 µm (5×). **(F)** Representative images and quantification of AT8 SI **(G)** and SS **(H)** tau oligomers and monomers from hippocampal lysates of NOX4$^{+/+}$ (GFP, n = 9 and hTau, n = 9) and NOX4$^{-/-}$ (GFP, n = 7 and hTau, n = 8) mice. **(I)** Imagens and quantification of AT180 SI **(J)** and SS **(K)** tau oligomers and monomers from hippocampal lysates of NOX4$^{+/+}$ (GFP, n = 5 and hTau, n = 5) and NOX4$^{-/-}$ (GFP, n = 5 and hTau, n = 5) mice. Data are presented as mean ± SEM. Significance was determined by one-way ANOVA with Tukey's post hoc test or Kruskal-Wallis with Dunn's post hoc test for nonparametric data sets. *p < 0.05; **p < 0.01; ***p < 0.001; #p < 0.05; ##p < 0.01.

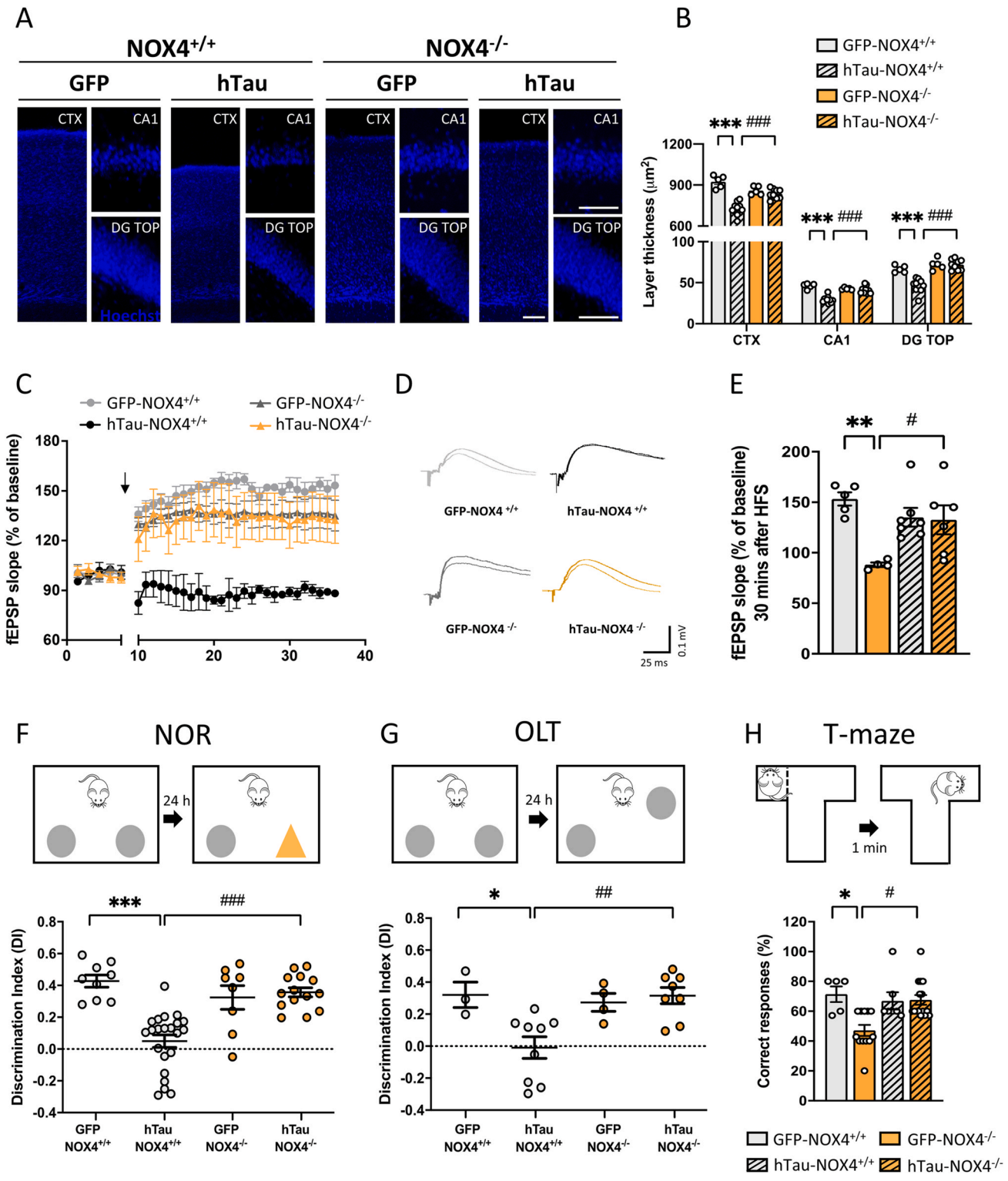

Fig. 2. NOX4 genetic deletion reduces hippocampal atrophy, improves LTP and cognitive deficits 28 days after hTau injection. **(A)** Representative images and **(B)** thickness quantification of CTX, CA1 and DG TOP in NOX4$^{+/+}$ (GFP, n = 5 and hTau, n = 10) and NOX4$^{-/-}$ (GFP, n = 5 and hTau, n = 9) mice. Scale bars: 100 μm (10×); 75 μm (40×). **(C)** *In vivo* long-term potentiation (LTP) in NOX4$^{+/+}$ and NOX4$^{-/-}$ mice injected with GFP or hTau over 30 min. Arrow indicates high-frequency stimulation (HFS). Five minutes of control period and 30 min after HFS stimulation are shown. **(D)** Representative traces before and after HFS. **(E)** Quantification of the fEPSP slope 30 min after HFS in NOX4$^{+/+}$ (GFP, n = 5 and hTau, n = 4) and NOX4$^{-/-}$ (GFP, n = 7 and AAV-hTau, n = 6) mice. **(F)** Quantification of the DI in the NOR test in NOX4$^{+/+}$ (GFP, n = 9 and hTau, n = 22) and NOX4$^{-/-}$ (GFP, n = 8 and hTau, n = 14) mice. **(G)** Quantification of the DI in OLT in NOX4$^{+/+}$ (GFP, n = 3 and hTau, n = 9) and NOX4$^{-/-}$ (GFP, n = 4 and hTau, n = 8) mice. **(H)** Quantification of the percentage of correct responses in the T maze in NOX4$^{+/+}$ (GFP, n = 5 and hTau, n = 12) and NOX4$^{-/-}$ (GFP, n = 7 and hTau, n = 15) mice. Data are presented as mean ± SEM. Significance was determined by one-way ANOVA with Tukey's post hoc test or Kruskal-Wallis with Dunn's post hoc test for nonparametric data sets. *p < 0.05; **p < 0.01; ***p < 0.001; #p < 0.05; ##p < 0.01; ###p < 0.001. CTX (Retrosplenial cortex); CA1 (pyramidal cell layer CA1 region); DG TOP (Dentate gyrus top layer); NOR (novel object recognition test); OLT (object location task); DI (discrimination index).

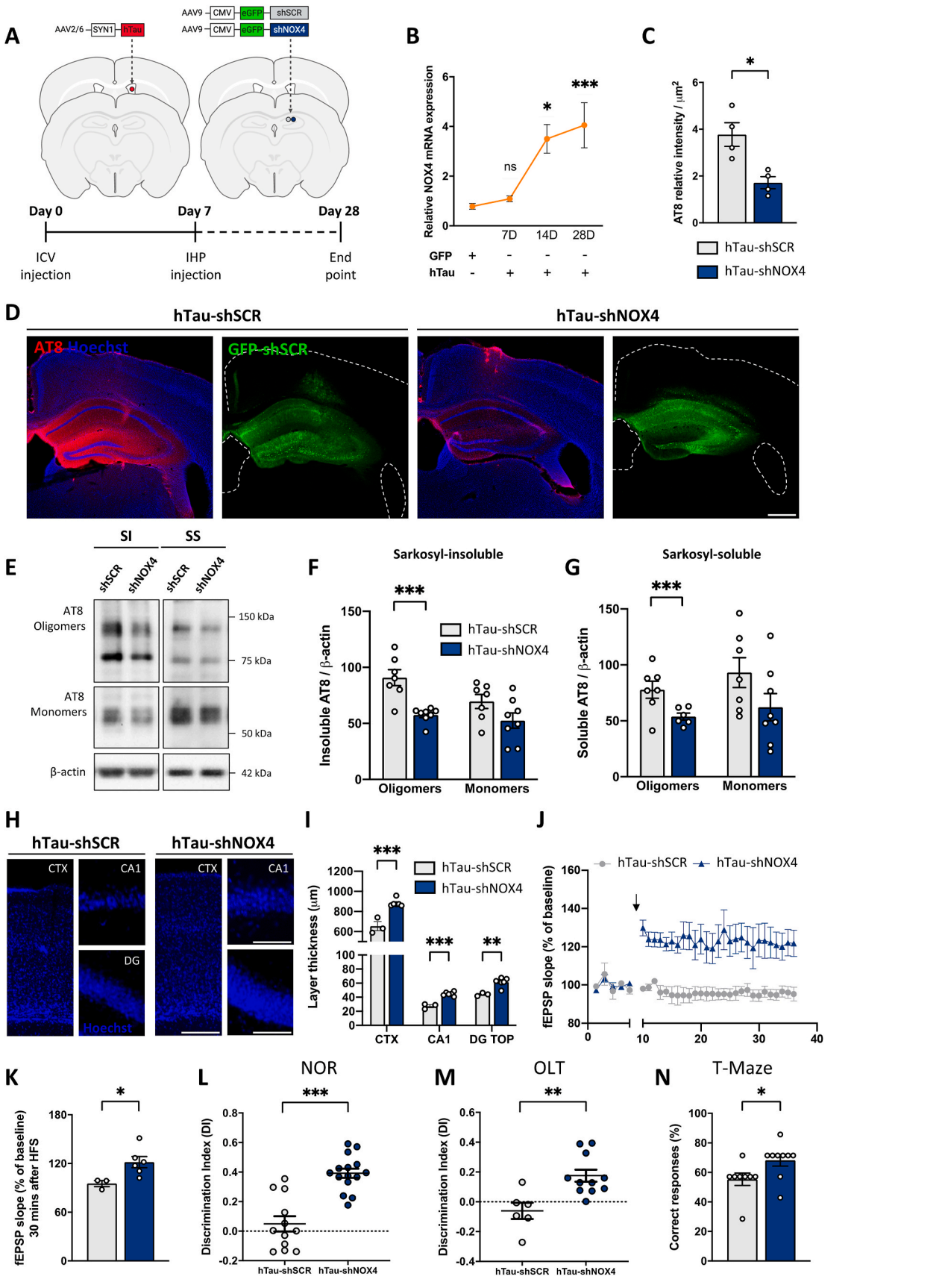

(caption on next page)

Fig. 3. Neuronal-targeted NOX4 knockdown diminishes the accumulation of hyperphosphorylated tau, improves LTP and cognitive decline once tauopathy is initiated. **(A)** Schematic representation of the protocol. **(B)** NOX4 mRNA from hippocampal lysates of NOX4$^{+/+}$ (GFP, n = 14 and hTau, n = 8) and NOX4$^{-/-}$ (GFP, n = 4 and hTau, n = 11) mice. **(C)** Quantification and **(D)** representative images of AT8 relative intensity in the hippocampus of hTau (shSCR, n = 4 and shNOX4, n = 4) mice. Scale bar: 500 μm (5×). **(E)** Representative images and quantification of AT8 **(F)** SI and **(G)** SS tau oligomers and monomers from hippocampal lysates of hTau (shSCR, n = 7 and shNOX4, n = 6–8) mice. Data are presented as mean ± SEM. Significance was determined by one-way ANOVA with Tukey's post hoc test or unpaired Student's *t*-test. *p < 0.05; ***p < 0.001. (**H**) Images and **(I)** quantification of the CTX, CA1, and DG TOP thickness in hTau (shSCR, n = 3 and shNOX4, n = 6) mice. Scale bars: 100 μm (10×); 75 μm (40×). **(J)** *In vivo* long-term potentiation (LTP) in hTau-shSCR and hTau-shNOX4 injected mice over 30 min. Arrow indicates high-frequency stimulation (HFS). Five minutes of control period and 30 min after HFS stimulation are shown. **(K)** Quantification of fEPSP slope. **(L)** DI in hTau (shSCR, n = 12 and shNOX4, n = 15) mice in the NOR test. **(M)** DI in hTau (shSCR, n = 6 and shNOX4, n = 11) mice in the OLT test. **(N)** Percentage of correct responses in hTau (shSCR, n = 8 and shNOX4, n = 9) in the T maze maze. Data show mean ± SEM. Significance was determined by unpaired Student's *t*-test or Mann-Whitney test for nonparametric data sets. *p < 0.05; **p < 0.01; ***p < 0.001. SI (sarkosyl-insoluble); SS (sarkosyl-soluble); CTX (Retrosplenial cortex); CA1 (pyramidal cell layer CA1 region); DG TOP (Dentate gyrus top layer); fEPSP (fast excitatory postsynaptic potential); DI (Discrimination Index); NOR (novel object recognition test); OLT (object location task).

Statistical significance was set at *p < 0.05; **p < 0.01; ***p < 0.001 in accordance to GP style.

2.15. Data availability

The authors declare that the data supporting the findings of this study are available within the article and its Supplemental data.

3. Results

3.1. NOX4 deletion reduces tau-driven pathology in an in vivo tauopathy model

ICV stereotaxic delivery of AAVs containing hTau^{P301L} (**hTau**) or GFP (**GFP**) was performed in NOX4$^{+/+}$ and NOX$^{-/-}$ mice (Fig. 1A); 28 days post-infection there was a significant increase of NOX4 mRNA in the ipsilateral hippocampus of hTau mice (4-fold) but not of other NOX isoforms (Fig. 1B). In addition, NOX4 immunofluorescence analysis revealed 1.9-fold increase of NOX4 in hippocampal CA1 neurons but not in astrocytes or microglial cells of hTau mice (Fig. 1C and Supplemental Fig. 2). AT8 immunoreactivity, which recognizes a pathologic hyperphosphorylated epitope of tau protein (pSer202/Thr205) and constitutes the basis of Braak staging [36], was increased (1.9-fold) in hTau-NOX4$^{+/+}$ mice; this increase was abrogated in hTau-NOX4$^{-/-}$ mice (Fig. 1D and E). We also measured the oligomers (from 75 to 250 kDa) and monomers (from 50 to 65 kDa) [37] of pathological hyperphosphorylated tau using a separation protocol on hippocampal homogenates to separate SI from SS fractions. Although no significant changes were observed in AT8 monomers, AT8 SI and SS oligomers were significantly increased in hTau-NOX4$^{+/+}$ mice and this increase was abolished in NOX4$^{-/-}$ mice (Fig. 1F–H). However, monomers and oligomers of AT180 (pThr231) in SI and SS fractions were all drastically reduced in hTau-NOX4$^{-/-}$ mice (Fig. 1I–K).

As pathogenic tau mediates neurodegeneration and synaptic dysfunction in tauopathy/AD models [38–40], we first measured the thickness of different layers in the hippocampus as an indication of neurotoxicity. hTau-NOX4$^{+/+}$ animals showed a reduction in the thickness of different areas of the hippocampus and this atrophy was prevented in hTau-NOX4$^{-/-}$ mice (Fig. 2A and B). Second, we performed LTP *in vivo* measurements which assesses synaptic plasticity and is used as a cellular model for learning and memory. Both, GFP-NOX4$^{+/+}$ and GFP-NOX4$^{-/-}$ injected mice presented sustained hippocampal LTP over 30 min. hTau-NOX4$^{+/+}$ mice exhibited LTP deficits while hTau-NOX4$^{-/-}$ did not (Fig. 2C–E). These results mirrored those obtained in different behavioral tasks related to memory acquisition, such as the NOR (Fig. 2F), the OLT (Fig. 2G) and the T-maze (Fig. 2H); hTau-NOX4$^{-/-}$ performed better than their hTau-NOX4$^{+/+}$ counterparts. Taken together, the absence of NOX4 in hTau mice reduces oligomeric pathological hyperphosphorylated tau, attenuates brain atrophy, and prevents LTP impairment and cognitive decline.

3.2. Selective neuronal NOX4 knockdown alleviates pathological-tau related alterations once tauopathy is initiated

To elucidate if neuronal NOX4 was the main driver in the reduction of tau-related pathology, 7 days after ICV hTau injection, AAVs encoding shRNA against neuronal NOX4 (shNOX4) or scramble shRNA (shSCR) used as control, were intrahippocampal delivered (Fig. 3A). At this timepoint, NOX4 mRNA was still not increased (Fig. 3B), although neuroinflammation, autophagy dysregulation and increased phosphorylated tau is present, but cognitive decline in not detected [30]. Both AAVs shSCR and shNOX4 contained GFP, which enabled their visualization predominantly in CA1 neurons (Supplemental Fig. 3A and B). In hTau-shNOX4 mice, NOX4 mRNA was decreased by 61% (Supplemental Fig. 3C) and protein levels of NOX4 visualized by immunofluorescence were reduced to similar levels of those observed in basal conditions (Supplemental Fig. 1C). Related to tau, AT8 was reduced by 55% in the ipsilateral hippocampus (Fig. 2C and D); while AT8 SI and SS oligomers were significantly reduced, no changes were observed in AT8 SI or SS monomers (Fig. 3E–G). AT180 oligomers and monomers of SI fractions were significantly reduced in hTau-shNOX4 mice, while SS oligomers and monomers remained unaltered (Supplemental Fig. 4A-C).

To assess whether knockdown of neuronal NOX4 affects tau-related neurotoxicity, we measured the thickness of CTX, CA1 and DG TOP. Neuronal-targeted NOX4 knockdown significantly decreased the atrophy observed in hTau-shSCR injected mice (Fig. 3H and I). Moreover, while hTau mice injected with control shSCR exhibited LTP deficiency, shNOX4 mice showed sustained and significant LTP over 30 min (Fig. 3J and K). This result correlated with the results achieved in the cognitive behavioral tests; discrimination indexes (DIs) in the NOR and OLT tests and the percentage of correct responses in the T test achieved in hTau-shNOX4 mice where significantly higher when compared with the hTau control mice (Fig. 3L and N). These results demonstrate that neuronal NOX4 knockdown is sufficient to alleviate tau-related alterations, even when tauopathy is initiated.

3.3. Impact of NOX4 absence on the ALP in vivo

As global or neuronal NOX4 deficiency reduced the accumulation of pathological oligomeric hyperphosphorylated tau, we sought of interest to evaluate the performance of macroautophagy, a highly characterized proteolysis pathway involved in the clearance of tau [5,7] in our mice. Following the experimental protocol in Fig. 1A, the macroautophagy markers p62 and microtubule-associated protein 1 light chain 3 (LC3) were accumulating in CA1 neurons of hTau-NOX4$^{+/+}$ mice (Fig. 4A–D), indicating a macroautophagy dysregulation. However, both global NOX4$^{-/-}$ (Fig. 4A–D) or neuronal NOX4 knockdown significantly reduced tau-driven p62 and LC3 accumulation (Fig. 4E–G). These results were corroborated by western bot (Supplemental Fig. 5A-C and H-J). However, in AAV-hTau injected mice, the absence of NOX4 did not changed p62 and LC3 mRNA levels, suggesting a post-transcriptional regulation of this clearance process (Supplemental Fig. 5D and E).

hTau-NOX4$^{-/-}$ mice presented enhancement of a key regulator of

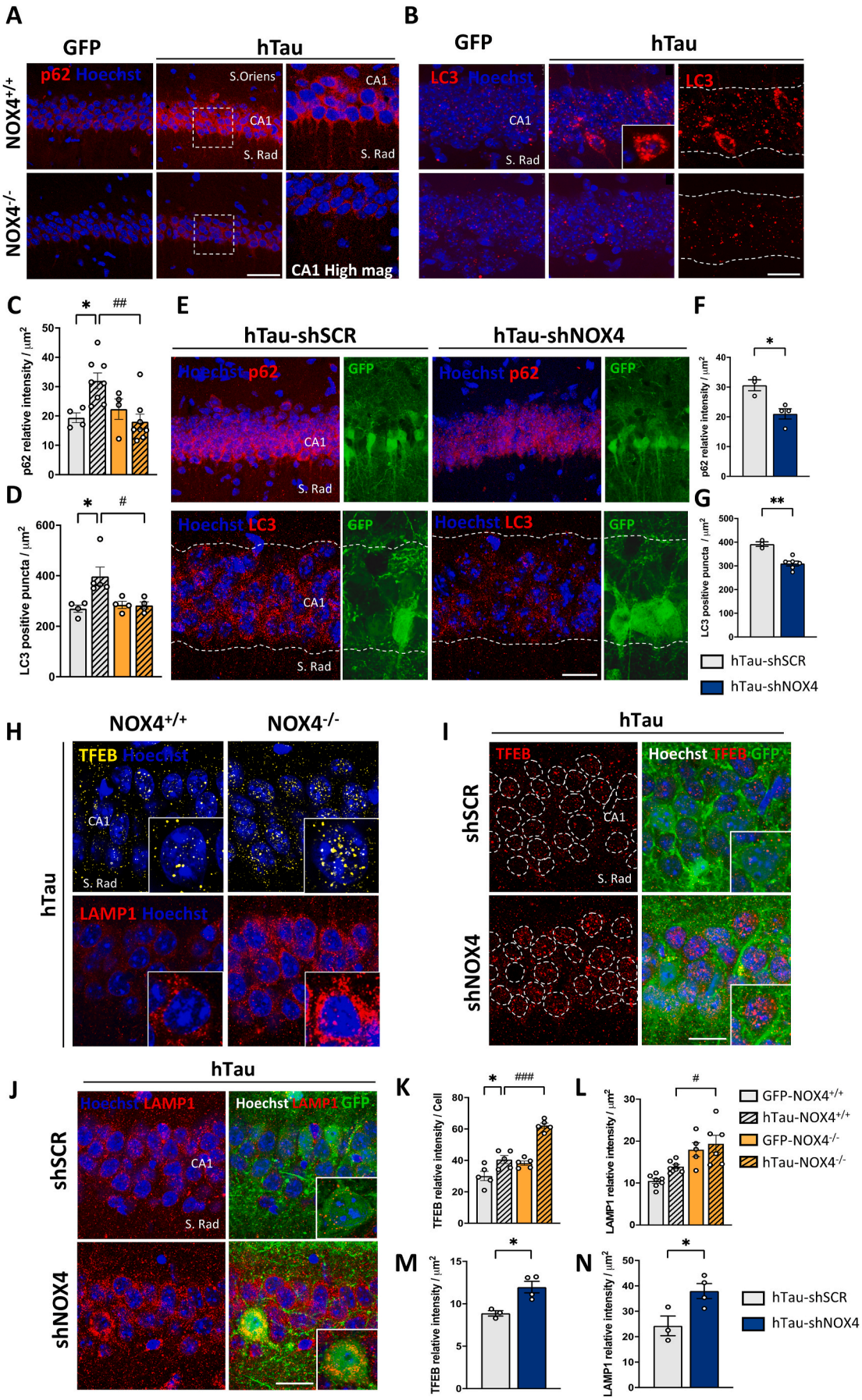

(caption on next page)

Fig. 4. Macroautophagy blockade induced by hTau injection is prevented in NOX4$^{-/-}$ and shNOX4 mice. **(A)** Representative images and **(C)** quantification of p62 relative intensity in the hippocampal CA1 region from NOX4$^{+/+}$ (GFP, n = 4 and hTau, n = 8) and NOX4$^{-/-}$ (GFP, n = 4 and hTau, n = 8) mice. Insets show images at a higher magnification. Scale bar: 25 μm (40×). **(B)** Representative images and **(D)** quantification of LC3 positive puncta in the hippocampal CA1 region from NOX4$^{+/+}$ (GFP, n = 4 and hTau, n = 5) and NOX4$^{-/-}$ (GFP, n = 4 and hTau, n = 4) mice. Scale bar: 15 μm (63×). **(E)** Representative images of p62 and LC3 and quantification of p62 **(F)** and LC3 **(G)** of hTau shSCR and shNOX4 mice (GFP, n = 3 and hTau, n = 4–6). **(H)** Representative images and quantification **(K, L)** of nuclear TFEB and LAMP1 relative intensity in the hippocampal CA1 region in NOX4$^{+/+}$ (GFP, n = 5–6 and hTau, n = 5) and NOX4$^{-/-}$ (GFP, n = 4–5 and hTau, n = 4–6). Insets show images at higher magnification. Scale bar: 15 μm (63×). **(I, J)** Representative images of TFEB and LAMP1 in hTau-shSCR and hTau-shNOX4 mice and its **(M,N)** quantification (hTau-shSCR, n = 3 and hTau-shNOX4, n = 3). Data are presented as mean ± SEM. Significance was determined by one-way ANOVA with Tukey's post hoc test. *p < 0.05; **p < 0.01; #p < 0.05; ##p < 0.01; ###p < 0.001. CA1 (pyramidal cell layer CA1 region); S.Oriens (Stratum Oriens); S.Rad (Stratum Radiatum).

lysosomal biogenesis, the nuclear transcription factor EB (TFEB) [41] in CA1 neurons (Fig. 4H and K); this effect was also observed in shNOX4 (Fig. 4I and M). This increase was accompanied by an increase of LAMP1, a target gene of TFEB, in hTau-NOX4$^{-/-}$ (Fig. 4H and L and Supplemental Fig. 5A and F) and in hTau-shNOX4 mice (Fig. 4J and N, and Supplemental Fig. 5H and K). Cathepsin D (CTSD), another target gene of TFEB, was also increased in the absence of global or neuronal NOX4 (Supplemental Fig. 5A, G, H and L).

Taken together, these results indicate that neuronal NOX4 knockdown is sufficient to prevent the macroautophagy blockade secondary to hTau and increases the expression of lysosomal-related proteins, unveiling NOX4 as a potential modulator of the lysosomal pathway, even when tauopathy is initiated. In addition to the protein aggregation and clearance imbalance, oxidative stress and inflammation are known to play a pivotal role in the progression of tauopathies [10,42,43]. Furthermore, NOX-derived ROS are essential signals to regulate autophagy [18,19]. Thus, we assessed whether NOX4 genetic deletion could modulate ROS production and inflammation secondary to hTau injection. While in hippocampi of hTau-NOX4$^{+/+}$ mice, ROS production and inflammatory-related markers were increased, in hTau-NOX4$^{-/-}$ mice they were reduced to control levels (Supplemental Fig. 6). These results highlight a key role of NOX4 in modulating ROS production and neuroinflammation in the humanized *in vivo* tauopathy model.

3.4. The absence of NOX4 in neuronal cultures reduces hyperphosphorylation of tau, prevents dendritic spine loss and modulates the ALP

To support the results obtained *in vivo*, primary neurons from NOX4$^{+/+}$ and NOX4$^{-/-}$ mice were cultured. At day 14, neurons were subjected to PBS (as control) or AAV-hTau (to reproduce the tauopathy *in vitro*) for 8 days (Fig. 5A). Under these experimental conditions, the number of AT8 positive neurons (Fig. 5B and C) and AT8 immunoreactivity per cell (Fig. 5D) were significantly decreased by 54% and 46%, in hTau-NOX4$^{-/-}$ *vs* hTau-NOX4$^{+/+}$ neurons, respectively. Hyperphosphorylated tau can be redirected from the axonal to the somatodendritic compartment where it can impair synaptic function and cause spine loss [44,45]; related to this, NOX4$^{+/+}$ neurons subjected to hTau showed 5 different patterns of AT8 staining throughout the dendritic compartment (Supplemental Fig. 7A). Interestingly, we observed a significant negative correlation between number of dendritic spines and hyperphosphorylated tau; as AT8 staining in dendrites increased, the number of dendritic spines decreased (Supplemental Fig. 7B). We also detected a qualitative reduction in AT8 somatodendritic missorting and a significant decrease in AT8 staining in dendrites in hTau-NOX4$^{-/-}$ neurons (Fig. 5E and Supplemental Fig. 7C); as expected, this was accompanied by an increase in the number of dendritic spines (Fig. 5F and G). Overall, these results correlate with those described *in vivo* indicating that the absence of NOX4 in neurons is sufficient to reduce the accumulation of pathologic hyperphosphorylated tau and suggests that a decrease in the mislocalization of hyperphosphorylated tau to the somatodendritic compartment, may prevent hTau-mediated dendritic spines loss in NOX4$^{-/-}$ neurons.

We also evaluated the macroautophagy markers p62 and LC3 by immunofluorescence in primary cultured neurons (Supplemental Fig. 8A–C); these proteins accumulated in hTau-NOX4$^{+/+}$ neurons, indicating a blockade in macroautophagy flux. By transducing primary neurons with a tandem reporter consisting of recombinant RFP and GFP fused to LC3 protein 48 h before the end point [46] (Fig. 5H) we confirmed an enhancement of the macroautophagy flux in hTau-NOX4$^{-/-}$ neurons. Thus, hTau-NOX4$^{+/+}$ neurons had a predominance of autophagosomes (AP) and fewer autophagolysosomes (APL), while hTau-NOX4$^{-/-}$ neurons showed the opposite effect, they had less AP and a higher number of APL (Fig. 5I and J). Moreover, analysis of TFEB, LAMP1 and CTSD in hTau primary cultured neurons provided similar results to those obtained *in vivo* (Fig. 5K-P). These findings, correlate with the significant co-localization of CTSD with AT8 (Fig. 5M and Q), indicating accumulation of pathological tau in lysosomes. These observations support the potential implication of NOX4 in regulating ALP in primary cultured neurons and explain, at least in part, the facilitation of the macroautophagy flux, to reduce accumulation of pathological tau, when NOX4 is absence.

3.5. NOX4 is overexpressed in patients with FTLD and AD

Finally, to examine whether NOX4 was implicated in human tauopathies, we analyzed post-mortem brain samples obtained from individuals that suffered FTLD or AD. In FTLD patients, only NOX4 mRNA levels were significantly increased by 2.8-fold (Fig. 6A, left panel), whereas in AD patients, both NOX2 (3.2-fold) and NOX4 (2.2-fold) mRNA were significantly increased when compared to non-demented subjects (Ctrl) (Fig. 6A, right panel). NOX4 protein levels in the hippocampus and prefrontal cortex, regions known to be affected during tauopathy progression, were significantly increased in both FTLD (3.1 and 2.1-fold respectively) and AD patients (2.4 and 1.5-fold respectively), compared to non-demented subjects (Fig. 6B and C). NOX4 protein levels correlated with mRNA levels, which were significantly increased in the hippocampus and prefrontal cortex of both types of tauopathies (Supplemental Fig. 9A). These changes were further supported by immunofluorescence analysis of fixed postmortem brain sections of FTLD and AD patients that revealed increased levels of NOX4 in hippocampal neurons positive for AT8 (Fig. 6D). Furthermore, AT8 SI oligomers and monomers were significantly augmented in FTLD (Fig. 6E and F) and AD (Fig. 6E and G) patients compared to Ctrl subjects. However, no significant changes were observed in AT8 SS forms (Supplemental Fig. 9B and C).

These data show an altered expression pattern of NOX4 in different brain areas of FTLD and AD patients in which insoluble forms of hyperphosphorylated tau are enriched, delineating a potential association between NOX4 and tau pathology in human tauopathies.

4. Discussion

Our results demonstrate that NOX4 expression is upregulated in the presence of pathological hyperphosphorylated tau in brains of AD and FTLD patients and in a humanized mouse model of tauopathy. Interestingly, either global knockout or neuronal-targeted knockdown of the *Nox4* gene in mice was able to: 1) reduce the levels of pathological hyperphosphorylated tau, 2) modulate macroautophagy, 3) reduce ROS and inflammation and 4) prevent brain atrophy and synaptic

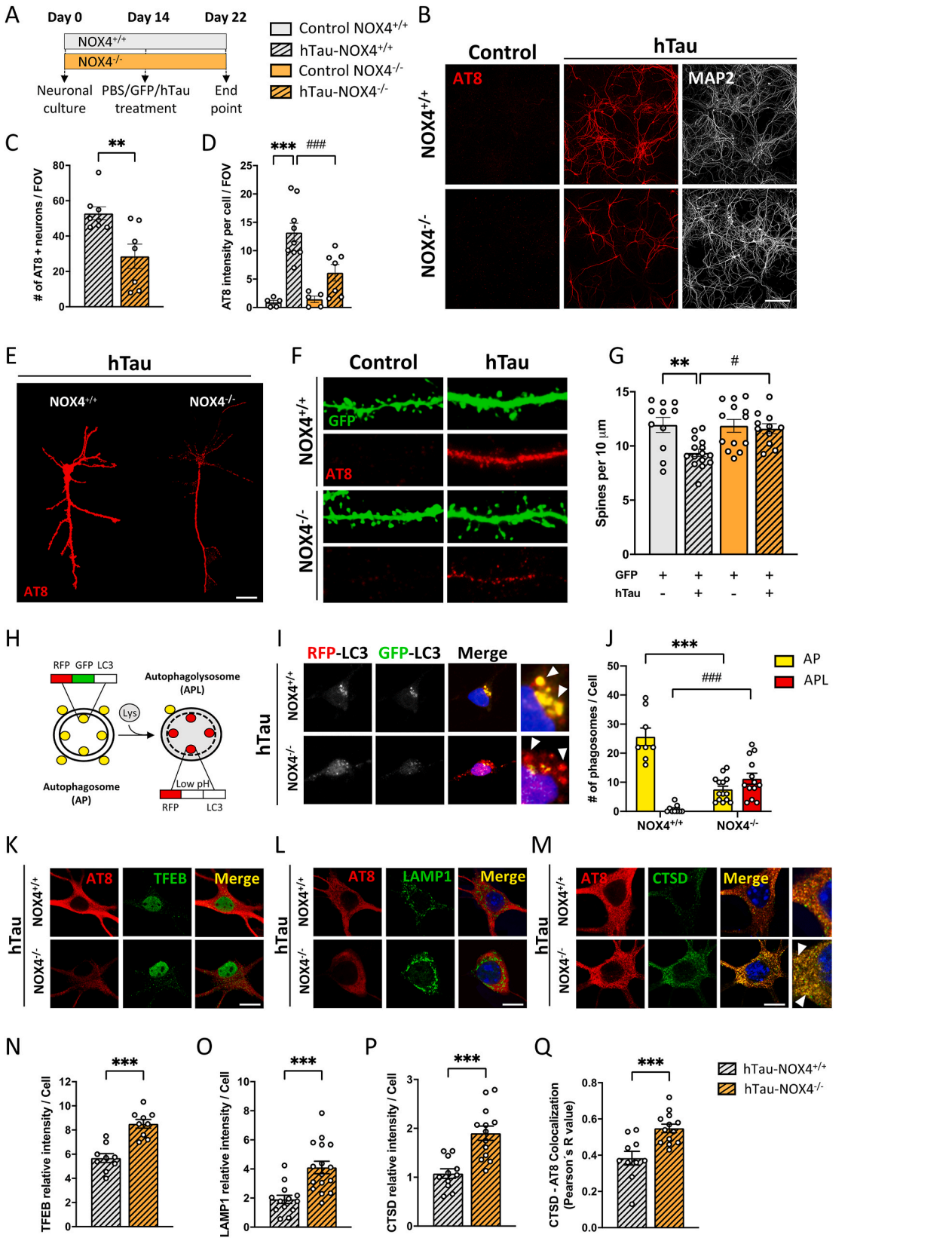

(caption on next page)

Fig. 5. NOX4 deficiency reduces AT8, prevents dendritic spine loss and avoids macroautophagy blockade in primary cultured neurons subjected to hTau. **(A)** Schematic representation of the protocol. **(B)** AT8 and MAP2 staining, **(C)** quantification of AT8 positive neurons and **(D)** AT8 immunoreactivity per cell in NOX4$^{+/+}$ (Control, n = 5 and hTau, n = 8–9) and NOX4$^{-/-}$ (Control, n = 5 and hTau, n = 7) neurons. Scale bar: 100 μm (20×). n = Field of view analyzed per condition from 3 independent experiments. **(E)** Images of AT8 somatodendritic missorting in hTau-NOX4$^{+/+}$ and hTau -NOX4$^{-/-}$ neurons. Scale bars: 20 μm (63×). **(F)** Images and **(G)** number of dendritic spines per 10 μm in the secondary and tertiary segments in NOX4$^{+/+}$ (GFP, n = 14 and GFP + hTau, n = 15) and NOX4$^{-/-}$ (GFP, n = 13 and GFP + hTau, n = 11) neurons. Scale bars: 5 μm (63×). n = neurons analyzed from 4 independent experiments. Significance was determined by one-way ANOVA with Tukey's post hoc test. **p < 0.01; #p < 0.05. Data are presented as mean ± SEM. **(H)** Representation of the RFP-GFP-LC3 tandem reporter. **(I)** Images and **(J)** quantification of the number of autophagosomes (AP) and autophagolysosomes (APL) per cell in hTau-NOX4$^{+/+}$ (n = 8–9) and hTau-NOX4$^{-/-}$ (n = 14–15) neurons transduced with the RFP-GFP-LC3 tandem reporter. Insets show images at a higher magnification. Arrows indicate autophagic vacuoles. Scale bar: 5 μm (63×). n = 3 independent experiments. Images of nuclear TFEB **(K)**, LAMP1 **(L)** and CTSD **(M)** relative intensity in hTau-NOX4$^{-/-}$ and hTau-NOX4$^{+/+}$ neurons. Insets show images at higher magnification. Arrows indicate co-localization. Scale bar: 5 μm (63×). Quantification of nuclear TFEB **(N)**, LAMP1 **(O)** and CTSD **(P)** relative intensity in hTau-NOX4$^{+/+}$ (n = 9–13) and hTau-NOX4$^{-/-}$ (n = 9–16) neurons. **(Q)** Quantification of CTSD-AT8 Pearson's R value in hTau-NOX4$^{+/+}$ (n = 10) and hTau-NOX4$^{-/-}$ (n = 13) neurons. Significance was determined by one-way ANOVA with Tukey's post hoc test or unpaired Student's *t*-test. ***p < 0.001; ###p < 0.001.

dysfunction, which translate into prevention of cognitive decline *in vivo*.

Although brain expression of NOX4 is low when compared with high expressing tissues like the kidney, being the brain an organ with high sensitivity to oxidative stress, subtle increases in ROS can have a major impact in brain function [47]. Kleinschnit et al. demonstrated that although NOX4 was barely detectable in healthy brain regions, clear positive labeling of NOX4 was seen in neurons and vascular endothelial cells from the forebrain cortex of stroke patients [29]. Furthermore, we have previously elucidated the superior sensitivity of the brain to ischemic damage at the cellular level by NOX4-dependent neuronal autotoxicity [22]. In addition, NOX4 immunoreactivity co-localizes in neurons in the injured cerebral cortex following TBI [24] and is upregulated in dopaminergic neurons of patients with PD [48]. Consequently, all these evidences support that although NOX4 expression in the healthy brain is low, it can be overexpressed under pathological conditions contributing to the progression of neurodegenerative diseases.

A robust correlation between the activity of NOX isoforms and cognitive decline was reported in AD patients and in the APPxPS1 mouse model [21,26,49]. In human brain samples we have observed that NOX2, which is predominantly expressed in microglia [50,51], was only increased in AD, as previously reported [52]. However, NOX4, whose expression is mostly neuronal [29,53], was upregulated in both FTLD and AD patients, suggesting a correlation between NOX4 and tau pathology. However, the potential contribution of NOX2 in tauopathies such as AD should not be neglected, since the results in AD patients also show a high expression of NOX2.

Interestingly, the results related to NOX4 expression in FTLD and AD human brain samples correlated with those found in the humanized *in vivo* tauopathy model, where NOX4 overexpression was preferentially restricted to the neuronal compartment and suggests that NOX4 may be upregulated in this cell type in response to hyperphosphorylated tau, while NOX2 could be more related to the microglial response to amyloidopathy [8,54]. This assumption was supported by the finding that not only global, but also neuronal NOX4 blockade, reduced the levels of pathological hyperphosphorylated tau oligomers, which were significantly increased in SI fractions of FTLD and AD patients, as well as in the SI and SS fractions in the *in vivo* tauopathy model. These oligomeric tau forms, which are present in the brain at early stages of AD [55,56], are described to be the most toxic species in tauopathies and are implicated in tau spreading [57–59]. We also found that the missorting of hyperphosphorylated tau towards the somatodendritic compartment, which causes synaptic dysfunction [44,45] was reduced in NOX4 deficient neurons. There was also an improvement in the number of dendritic spines when NOX4 was abolished. These results, together with the reduction of hyperphosphorylated pathologic forms of tau, further contribute to explain the reduction in brain atrophy, the improvement in synaptic dysfunction (LTP) and cognitive impairment (NOR, OLT and T-maze) when total or neuronal NOX4 was knocked down in hTau mice. Altogether, these results indicate a beneficial effect of NOX4 blockade in tauopathy.

In order to explain a causal role of NOX4 in tau pathology, we focused on autophagy which is one of the degradative pathways to eliminate hyperphosphorylated tau, besides the proteasome [7,60]. Also, because ROS, which are produced by NOXs, have been described as essential signals to activate autophagy [15,41]. In particular, NOX4 has consistently shown to induce the autophagy process [18,61]. Our results evidence that NOX4 deficiency reduces ROS production. Thus, we hypothesize that NOX4-derived ROS may participate in the over-induction of macroautophagy which, together with the toxic effect exerted by hTau^{P301L} on this degradative mechanism, could determine the defective performance of this pathway, the excessive accumulation of autophagosomes [62,63] and the faulty degradation of pathological forms of tau, in consistence with what has been described in several NDDs [6]. Our results show that neuronal-targeted NOX4 knockdown, prevents macroautophagy blockade, even when tau-related alterations were initiated. Furthermore, NOX4 deficiency increased the number of functional acidic autophagolysomes, restoring the macroautophagy flux. These results suggest that an increase of neuronal NOX4 in tauopathy could play an active role in dysregulating macroautophagy flux and, thereby, contributing to disease progression. In AD patients, increased induction of macroautophagy causes an overburden of failing lysosomes that lead to neuronal toxicity, pinpointing the progressive decline of lysosomal clearance as a facilitator of the robust autophagy pathology and neuritic dystrophy implicated in AD pathogenesis [11,64–66]. Hereof, TFEB is a transcription factor that coordinately activates the expression of key genes that regulate lysosomal biogenesis and functionality and modulates genes required for autophagosome formation [67]. Recent studies suggest that increasing TFEB expression could be beneficial for the treatment of AD and other tauopathies [68,69]. In this study, NOX4 genetic deletion and neuronal-targeted NOX4 knockdown, augmented the nuclear localization of TFEB, together with the overexpression of its transcripts LAMP1 and CTSD. These findings can be interpreted as neuronal NOX4 downregulation can trigger TFEB nuclear translocation, increasing the availability of functional lysosomes to facilitate autophagosome degradation. In this regard, increased co-localization of AT8 tau in CTSD positive lysosomes in NOX4$^{-/-}$ neurons was identified, suggesting enhanced delivery of hyperphosphorylated tau to lysosomes for degradation. Altogether, these results correlate with the reduction of hyperphosphorylated tau forms and may explain the absence of cognitive decline in global and neuronal NOX4 knockdown mice.

In conclusion, this study validates NOX4 as a new and unexplored target for the treatment of tauopathies and highlights the potential clinical relevance of developing BBB-permeable specific NOX4 inhibitors for tau-mediated neurodegenerative disorders.

Author contributions

EL contributed to design and conduct research experiments, to acquire and analyze data and to write the manuscript. PTA contributed to conduct research experiments, to acquire and analyze data and to write

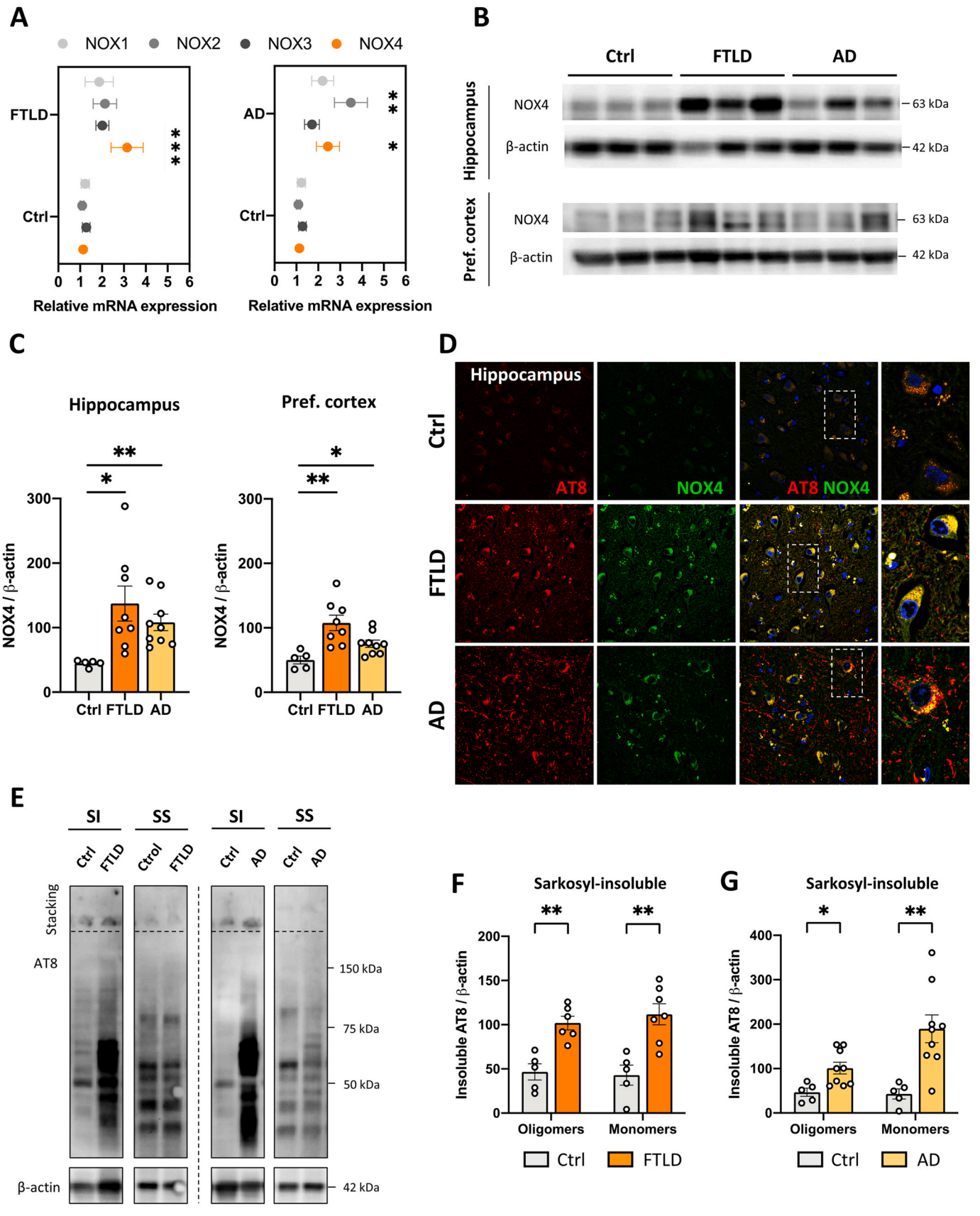

(caption on next page)

Fig. 6. NOX4 is overexpressed in brains of FTLD and AD patients. **(A)** mRNA levels of NOX isoforms in postmortem human brain lysates from FTLD (left) (n = 8), AD (right) (n = 9) and non-demented subjects (Ctrl) (n = 5). **(B)** Representative images and **(C)** quantification of NOX4 protein levels in hippocampus (left) and prefrontal cortex (right) from FTLD (n = 8), AD (n = 9) and Ctrl subjects (n = 5). **(D)** Representative images of AT8 and NOX4 intensity in fixed postmortem hippocampal sections of FTLD (n = 2), AD (n = 2) and Ctrl subjects (n = 2). Insets show images at a higher magnification. Scale bar: 25 μm. 3 fields of view were acquired per subject. **(E)** Representative images of AT8 SI and SS tau oligomers and monomers from hippocampal lysates of FTLD, AD and Ctrl subjects. **(F)** Quantification of AT8 SI tau oligomers and monomers from FTLD (n = 6–7) and Ctrl subjects (n = 5). **(G)** Quantification of AT8 SI tau oligomers and monomers from AD (n = 9) and Ctrl subjects (n = 5). Data are presented as mean ± SEM. Significance was determined by an unpaired Student's *t*-test or Mann-Whitney test for nonparametric data sets. *p < 0.05; **p < 0.01; ***p < 0.001. Ctrl (non-demented); FTLD (Frontotemporal lobar degeneration); AD (Alzheimer's disease); SI (sarkosyl-insoluble); SS (sarkosyl-soluble).

the manuscript. CFM contributed to conduct research experiments. AN, CP, NG, MDC, and SS contributed to perform experiments. CS and JB provided the AAV. PN provided technical advice. AR and JH provided patient samples. AIC and HHHWS provided mice colonies. MGL contributed to the design of the study, provided resources and to the writing of the manuscript. EL, PTA, CFM, MDC, HHHWS and MGL reviewed and edited the manuscript.

Funding

This study was supported by the Spanish ministry of science, innovation and universities Ref. RTI2018-095793-B-I00 and the General Council for Research and Innovation of the Community of Madrid and European Structural Funds Ref. B2017/BMD-3827 – NRF24ADCM to MGL. EL has a fellowship from Fundación Tatiana Pérez de Guzmán el Bueno. PTA and CFM have fellowships, Ref. FPU16/03239 and FPU15/03260 respectively, from the Spanish ministry of science, innovation and universities.

Declaration of competing interest

There are no competing interests.

Acknowledgements

We would like to thank Fundación Teófilo Hernando for its continuous support. All schemes were created with Biorender.com.

Appendix A. Supplementary data

Supplementary data related to this article can be found at https://doi.org/10.1016/j.redox.2021.102210.

References

[1] C. Li, J. Götz, Tau-based therapies in neurodegeneration: opportunities and challenges, Nat Rev Drug Discov 16 (2017) 863–883.
[2] Y. Wang, E. Mandelkow, Degradation of tau protein by autophagy and proteasomal pathways, Biochem. Soc. Trans. 40 (2012) 644–652. Biochem Soc Trans.
[3] F.M. Menzies, A. Fleming, A. Caricasole, C.F. Bento, S.P. Andrews, A. Ashkenazi, et al., Autophagy and neurodegeneration: pathogenic mechanisms and therapeutic opportunities, Neuron 93 (2017) 1015–1034.
[4] D.J. Klionsky, Y. Ohsumi, Vacuolar import of proteins and organelles from the cytoplasm, Annu Rev Cell Dev Biol 15 (1999) 1–32.
[5] R.A. Nixon, D.S. Yang, J.H. Lee, Neurodegenerative lysosomal disorders: a continuum from development to late age, Autophagy 4 (2008) 590–599.
[6] B. Boland, W.H. Yu, O. Corti, B. Mollereau, A. Henriques, E. Bezard, et al., Promoting the clearance of neurotoxic proteins in neurodegenerative disorders of ageing, Nat Rev Drug Discov 17 (2018) 660–688.
[7] A. Scrivo, M. Bourdenx, O. Pampliega, A.M. Cuervo, Selective autophagy as a potential therapeutic target for neurodegenerative disorders, Lancet Neurol 17 (2018) 802–815.
[8] A. Carrano, J.J.M. Hoozemans, S.M. Van Der Vies, A.J.M. Rozemuller, J. Van Horssen, H.E. De Vries, Amyloid beta induces oxidative stress-mediated blood-brain barrier changes in capillary amyloid angiopathy, Antioxidants Redox Signal 15 (2011) 1167–1178.
[9] T. Hamano, T.F. Gendron, E. Causevic, S.H. Yen, W.L. Lin, C. Isidoro, et al., Autophagic-lysosomal perturbation enhances tau aggregation in transfectants with induced wild-type tau expression, Eur J Neurosci 27 (2008) 1119–1130.
[10] B. Caballero, Y. Wang, A. Diaz, I. Tasset, Y.R. Juste, B. Stiller, et al., Interplay of pathogenic forms of human tau with different autophagic pathways, Aging Cell 17 (2018).
[11] D.S. Yang, P. Stavrides, P.S. Mohan, S. Kaushik, A. Kumar, M. Ohno, et al., Therapeutic effects of remediating autophagy failure in a mouse model of Alzheimer disease by enhancing lysosomal proteolysis, Autophagy 7 (2011) 788–789.
[12] E.E. Congdon, E.M. Sigurdsson, Tau-targeting therapies for Alzheimer disease, Nat Rev Neurol 14 (2018) 399–415.
[13] J.M. Long, D.M. Holtzman, Alzheimer disease: an update on pathobiology and treatment strategies, Cell 179 (2019) 312–339.
[14] X. Wen, J. Wu, F. Wang, B. Liu, C. Huang, Y. Wei, Deconvoluting the role of reactive oxygen species and autophagy in human diseases, Free Radic Biol Med 65 (2013) 402–410.
[15] E.E. Essick, F. Sam, Oxidative stress and autophagy in cardiac disease, neurological disorders, aging and cancer, Oxid Med Cell Longev 3 (2010) 168–177.
[16] M. Dodson, V. Darley-Usmar, J. Zhang, Cellular metabolic and autophagic pathways: traffic control by redox signaling, Free Radic Biol Med 63 (2013) 207–221.
[17] H. Buvelot, V. Jaquet, K.H. Krause, Mammalian NADPH oxidases, Methods Mol. Biol. 1982 (2019) 17–36. Humana Press Inc.
[18] M. Forte, S. Palmerio, D. Yee, G. Frati, S. Sciarretta, Functional role of Nox4 in autophagy, Adv. Exp. Med. Biol. 982 (2017) 307–326. Springer New York LLC.
[19] S. Sciarretta, M. Volpe, J. Sadoshima, NOX4 regulates autophagy during energy deprivation, Autophagy 10 (2014) 699–701.
[20] S. Sorce, R. Stocker, T. Seredenina, R. Holmdahl, A. Aguzzi, A. Chio, et al., NADPH oxidases as drug targets and biomarkers in neurodegenerative diseases: what is the evidence? Free Radic Biol Med 112 (2017) 387–396.
[21] A.J. Bruce-Keller, S. Gupta, A.G. Knight, T.L. Beckett, J.M. McMullen, P.R. Davis, et al., Cognitive impairment in humanized APP×PS1 mice is linked to Aβ 1-42 and NOX activation, Neurobiol Dis 44 (2011) 317–326.
[22] A.I. Casas, E. Geuss, P.W.M. Kleikers, S. Mencl, A.M. Herrmann, I. Buendia, et al., NOX4-dependent neuronal autotoxicity and BBB breakdown explain the superior sensitivity of the brain to ischemic damage, Proc Natl Acad Sci U S A 114 (2017) 12315–12320.
[23] K. Belarbi, E. Cuvelier, A. Destée, B. Gressier, M.C. Chartier-Harlin, NADPH oxidases in Parkinson's disease: a systematic review, Mol Neurodegener 12 (2017).
[24] M.W. Ma, J. Wang, K.M. Dhandapani, D.W. Brann, Deletion of NADPH oxidase 4 reduces severity of traumatic brain injury, Free Radic Biol Med 117 (2018) 66–75.
[25] Z. Li, F. Tian, Z. Shao, X. Shen, X. Qi, H. Li, et al., Expression and clinical significance of non-phagocytic cell oxidase 2 and 4 after human traumatic brain injury, Neurol Sci 36 (2015) 61–71.
[26] M.A. Ansari, S.W. Scheff, NADPH-oxidase activation and cognition in Alzheimer disease progression, Free Radic Biol Med 51 (2011) 171–178.
[27] L. Park, P. Zhou, R. Pitstick, C. Capone, J. Anrather, E.H. Norris, et al., Nox2-derived radicals contribute to neurovascular and behavioral dysfunction in mice overexpressing the amyloid precursor protein, Proc Natl Acad Sci U S A 105 (2008) 1347–1352.
[28] W. Tao, L. Yu, S. Shu, Y. Liu, Z. Zhuang, S. Xu, et al., miR-204-3p/Nox4 mediates memory deficits in a mouse model of Alzheimer's disease, Mol Ther 29 (2021) 396–408.
[29] C. Kleinschnitz, H. Grund, K. Wingler, M.E. Armitage, E. Jones, M. Mittal, et al., Post-stroke inhibition of induced NADPH Oxidase type 4 prevents oxidative stress and neurodegeneration, PLoS Biol 8 (2010).
[30] E. Luengo, I. Buendia, C. Fernández-Mendívil, P. Trigo-Alonso, P. Negredo, P. Michalska, et al., Pharmacological doses of melatonin impede cognitive decline in tau-related Alzheimer models, once tauopathy is initiated, by restoring the autophagic flux, J Pineal Res 67 (2019).
[31] S. Castro-Sánchez, J. Zaldivar-Diez, E. Luengo, M.G. López, C. Gil, A. Martínez, et al., Cognitive enhancement, TAU phosphorylation reduction, and neuronal protection by the treatment of an LRRK2 inhibitor in a tauopathy mouse model, Neurobiol Aging 96 (2020) 148–154.
[32] M. Leger, A. Quiedeville, V. Bouet, B. Haelewyn, M. Boulouard, P. Schumann-Bard, et al., Object recognition test in mice, Nat Protoc 8 (2013) 2531–2537.
[33] B.C. Beckelman, W. Yang, N.P. Kasica, H.R. Zimmermann, X. Zhou, C.D. Keene, et al., Genetic reduction of eEF2 kinase alleviates pathophysiology in Alzheimer's disease model mice, J Clin Invest 129 (2019) 820–833.
[34] R.M.J. Deacon, J.N.P. Rawlins, T-maze alternation in the rodent, Nat Protoc 1 (2006) 7–12.
[35] B. Schürmann, D.P. Bermingham, K.J. Kopeikina, K. Myczek, S. Yoon, K.E. Horan, et al., A novel role for the late-onset Alzheimer's disease (LOAD)-associated protein Bin1 in regulating postsynaptic trafficking and glutamatergic signaling, Mol Psychiatry 25 (2020) 2000–2016.
[36] H. Braak, I. Alafuzoff, T. Arzberger, H. Kretzschmar, K. Tredici, Staging of Alzheimer disease-associated neurofibrillary pathology using paraffin sections and immunocytochemistry, Acta Neuropathol 112 (2006) 389–404.

[37] H.C. Tai, A. Serrano-Pozo, T. Hashimoto, M.P. Frosch, T.L. Spires-Jones, B. T. Hyman, The synaptic accumulation of hyperphosphorylated tau oligomers in alzheimer disease is associated with dysfunction of the ubiquitin-proteasome system, Am J Pathol 181 (2012) 1426–1435.
[38] B. Dejanovic, M.A. Huntley, A. De Mazière, W.J. Meilandt, T. Wu, K. Srinivasan, et al., Changes in the synaptic proteome in tauopathy and rescue of Tau-induced synapse loss by C1q antibodies, Neuron 100 (2018) 1322–1336.e7.
[39] L. Zhou, J. McInnes, K. Wierda, M. Holt, A.G. Herrmann, R.J. Jackson, et al., Tau association with synaptic vesicles causes presynaptic dysfunction, Nat Commun 8 (2017).
[40] S. Chatterjee, R. Cassel, A. Schneider-Anthony, K. Merienne, B. Cosquer, L. Tzeplaeff, et al., Reinstating plasticity and memory in a tauopathy mouse model with an acetyltransferase activator, EMBO Mol Med 10 (2018).
[41] M. Sardiello, M. Palmieri, A Di Ronza, D.L. Medina, M. Valenza, V.A. Gennarino, et al., A gene network regulating lysosomal biogenesis and function, Science 325 (2009) 473–477, 80-.
[42] M.M. Haque, D.P. Murale, Y.K. Kim, J.S. Lee, Crosstalk between oxidative stress and tauopathy, Int J Mol Sci 20 (2019).
[43] C. Laurent, L. Buée, D. Blum, Tau and neuroinflammation: what impact for Alzheimer's disease and tauopathies? Biomed J 41 (2018) 21–33.
[44] E. Thies, E.M. Mandelkow, Missorting of tau in neurons causes degeneration of synapses that can be rescued by the kinase MARK2/Par-1, J Neurosci 27 (2007) 2896–2907.
[45] B.R. Hoover, M.N. Reed, J. Su, R.D. Penrod, L.A. Kotilinek, M.K. Grant, et al., Tau mislocalization to dendritic spines mediates synaptic dysfunction independently of neurodegeneration, Neuron 68 (2010) 1067–1081.
[46] S. Kimura, T. Noda, T. Yoshimori, Dissection of the autophagosome maturation process by a novel reporter protein, tandem fluorescent-tagged LC3, Autophagy 3 (2007) 452–460.
[47] C. KS, Metabolite imaging: knock, nox-ROS there? Nat Chem Biol 7 (2011) 71–72.
[48] W.M. Zawada, R.E. Mrak, J.A. Biedermann, Q.D. Palmer, S.M. Gentleman, O. Aboud, et al., Loss of angiotensin II receptor expression in dopamine neurons in Parkinson's disease correlates with pathological progression and is accompanied by increases in Nox4- and 8-OH guanosine-related nucleic acid oxidation and caspase-3 activation, Acta Neuropathol Commun 3 (2015) 9.
[49] A.J. Bruce-Keller, S. Gupta, T.E. Parrino, A.G. Knight, P.J. Ebenezer, A.M. Weidner, et al., NOX Activity is increased in mild cognitive impairment, Antioxidants Redox Signal 12 (2010) 1371–1382.
[50] Y. Zhang, K. Chen, S.A. Sloan, M.L. Bennett, A.R. Scholze, S. O'Keeffe, et al., An RNA-sequencing transcriptome and splicing database of glia, neurons, and vascular cells of the cerebral cortex, J Neurosci 34 (2014) 11929–11947.
[51] D.W. Infanger, R.V. Sharma, R.L. Davisson, NADPH oxidases of the brain: distribution, regulation, and function, Antioxidants Redox Signal 8 (2006) 1583–1596.
[52] A. Wyssenbach, T. Quintela, F. Llavero, J.L. Zugaza, C. Matute, E. Alberdi, Amyloid β-induced astrogliosis is mediated by β1-integrin via NADPH oxidase 2 in Alzheimer's disease, Aging Cell 15 (2016) 1140–1152.
[53] P. Vallet, Y. Charnay, K. Steger, E. Ogier-Denis, E. Kovari, F. Herrmann, et al., Neuronal expression of the NADPH oxidase NOX4, and its regulation in mouse experimental brain ischemia, Neuroscience 132 (2005) 233–238.
[54] A. Carrano, J.J.M. Hoozemans, S.M. Van Der Vies, J. Van Horssen, H.E. De Vries, A. J.M. Rozemuller, Neuroinflammation and blood-brain barrier changes in capillary amyloid angiopathy, Neurodegener Dis 10 (2012) 329–331.
[55] C.A. Lasagna-Reeves, D.L. Castillo-Carranza, U. Sengupta, J. Sarmiento, J. Troncoso, G.R. Jackson, et al., Identification of oligomers at early stages of tau aggregation in Alzheimer's disease, FASEB J 26 (2012) 1946–1959.
[56] M.D.C. Cárdenas-Aguayo, L. Gómez-Virgilio, S. DeRosa, M.A. Meraz-Ríos, The role of tau Oligomers in the onset of Alzheimer's disease neuropathology, ACS Chem Neurosci 5 (2014) 1178–1191.
[57] S.S. Shafiei, M.J. Guerrero-Muñoz, D.L. Castillo-Carranza, Tau oligomers: cytotoxicity, propagation, and mitochondrial damage, Front Aging Neurosci 9 (2017).
[58] M. Goedert, M.G. Spillantini, Propagation of tau aggregates Tim Bliss, Mol Brain 10 (2017).
[59] L. Jiang, P.E.A. Ash, B.F. Maziuk, H.I. Ballance, S. Boudeau, A Al Abdullatif, et al., TIA1 regulates the generation and response to toxic tau oligomers, Acta Neuropathol 137 (2019) 259–277.
[60] J.H. Liang, J.P. Jia, Dysfunctional autophagy in Alzheimer's disease: pathogenic roles and therapeutic implications, Neurosci Bull 30 (2014) 308–316.
[61] R. Scherz-Shouval, E. Shvets, E. Fass, H. Shorer, L. Gil, Z. Elazar, Reactive oxygen species are essential for autophagy and specifically regulate the activity of Atg4, EMBO J 26 (2007) 1749–1760.
[62] J. Liu, L. Li, Targeting autophagy for the treatment of Alzheimer's disease: challenges and opportunities, Front Mol Neurosci 12 (2019).
[63] A. Barnett, G.J. Brewer, Autophagy in aging and Alzheimer's disease: pathologic or protective? J Alzheimer's Dis. 25 (2011) 385–394.
[64] M. Bordi, M.J. Berg, P.S. Mohan, C.M. Peterhoff, M.J. Alldred, S. Che, et al., Autophagy flux in CA1 neurons of Alzheimer hippocampus: increased induction overburdens failing lysosomes to propel neuritic dystrophy, Autophagy 12 (2016) 2467–2483.
[65] D.S. Yang, P. Stavrides, P.S. Mohan, S. Kaushik, A. Kumar, M. Ohno, et al., Reversal of autophagy dysfunction in the TgCRND8 mouse model of Alzheimer's disease ameliorates amyloid pathologies and memory deficits, Brain 134 (2011) 258–277.
[66] D.S. Yang, P. Stavrides, M. Saito, A. Kumar, J.A. Rodriguez-Navarro, M. Pawlik, et al., Defective macroautophagic turnover of brain lipids in the TgCRND8 Alzheimer mouse model: prevention by correcting lysosomal proteolytic deficits, Brain 137 (2014) 3300–3318.
[67] C.J. Cortes, A.R. La Spada, TFEB dysregulation as a driver of autophagy dysfunction in neurodegenerative disease: molecular mechanisms, cellular processes, and emerging therapeutic opportunities, Neurobiol Dis 122 (2019) 83–93.
[68] Q. Xiao, P. Yan, X. Ma, H. Liu, R. Perez, A. Zhu, et al., Neuronal-targeted TFEB accelerates lysosomal degradation of app, reducing A$β$ generation and amyloid plaque pathogenesis, J Neurosci 35 (2015) 12137–12151.
[69] H. Martini-Stoica, A.L. Cole, D.B. Swartzlander, F. Chen, Y.W. Wan, L. Bajaj, et al., TFEB enhances astroglial uptake of extracellular tau species and reduces tau spreading, J Exp Med 215 (2018) 2355–2377.